Using Heterogeneity to Predict Inhibitory Network Model Characteristics

*†‡F.K. Skinner[1], *J.Y.J. Chung, *I. Ncube,
*‡P.A. Murray, **S.A. Campbell

*Toronto Western Research Institute, University Health Network
†Depts. of Medicine (Neurology), Physiology and
‡Institute of Biomaterials and Biomedical Engineering,
University of Toronto, Toronto, Ontario, Canada
**Department of Applied Mathematics,
University of Waterloo, Waterloo, Ontario, Canada

[1]Please address correspondence to F. K. Skinner at Toronto Western Research Institute, University Health Network, 399 Bathurst St., MP13-317, Toronto, Ontario, CANADA M5T 2S8. Phone:416-603-5800x5107; FAX:416-603-5745; email:fskinner@uhnres.utoronto.ca

ABSTRACT

From modelling studies it has been known for over ten years that purely inhibitory networks can produce synchronous output given appropriate balances of intrinsic and synaptic parameters. Several experimental studies indicate that synchronous activity produced by inhibitory networks is critical to the production of population rhythms associated with various behavioural states. Heterogeneity of inputs to inhibitory networks strongly affect their ability to synchronize. In this paper, we explore how the amount of input heterogeneity to two-cell inhibitory networks affects their dynamics. Using numerical simulations and bifurcation analyses, we find that the ability of inhibitory networks to synchronize in the face of heterogeneity depends non-monotonically on each of the synaptic time constant, synaptic conductance and external drive parameters. Because of this, an optimal set of parameters for a given cellular model with various biophysical characteristics can be determined. We suggest that this could be a helpful approach to use in determining the importance of different, underlying biophysical details. We further find that two-cell coherence properties are maintained in larger ten-cell networks. As such, we think that a strategy of "embedding" small network dynamics in larger networks is a useful way to understand the contribution of biophysically-derived parameters to population dynamics in large networks.

1 Introduction

Interneurons, or inhibitory GABAergic cells in the hippocampus and cortex represent about 10-20% of the total neuronal population. They are known to be very diverse in terms of their biochemical content, morphology, electrophysiological characteristics and neuromodulator sensitivites [McBain and Fisahn, 2001]. Importantly, networks of these inhibitory cells have been found to be responsible for the generation and control of rhythmic brain acitivities, moulding the appropriate temporal output of pyramidal cells [Buzsáki and Chrobak, 1995, Freund and Buzsáki, 1996]. For example, oscillatory activity in the hippocampus in the theta (8-12 Hz) and gamma (20-80 Hz) frequency bands occur during memory consolidation and spatial navigation [Bragin et al., 1995, Buzsáki, 2002]. Several experimental studies indicate that population (network) rhythms arise as a result of coherent activities in interneurons (e.g., [Traub et al., 1999, Whittington et al., 1995, Wu et al., 2002]). Extensive work on interneurons in recent years is giving rise to well-defined characteristics of interneurons with potential functional significance. For example, parvalbumin-containing basket cells seem to make up a relatively unmodifiable inhibitory network population responsible for generating gamma and theta rhythms [Freund, 2003]. To understand the generation and control of population rhythms, we need to know what are the important controlling factor(s) (i.e., biophysical constraints) or cellular mechanism(s) underlying interneuron coherence.

It was over a decade ago that modelling studies showed that it is possible to obtain synchronous output from purely inhibitory networks [Wang and Rinzel, 1992]. Since then, several modelling and theoretical studies of inhibitory networks have been performed (e.g., [Skinner et al., 1994, vanVreeswijk et al., 1994, Wang and Rinzel, 1993]). The inclusion of heterogeneous inputs to inhibitory networks has been considered in later studies [Bartos et al., 2001, Bartos et al., 2002, Maex and De Schutter, 2003, Neltner et al., 2000, Tiesinga and José, 2000, Wang and Buzsáki, 1996, White et al., 1998], and from them, it is clear that heterogeneity is a significant factor that strongly affects the ability of inhibitory networks to synchronize. However, an exploration of how much heterogeneity can be tolerated by inhibitory networks under a range of synaptic conductance and time constant conditions has not been done. This is an important consideration since recent work by Bartos and colleagues (2001, 2002), in which inhibitory synaptic characteristics were directly measured, showed that the decay time constants were smaller (< 5 ms) than what is typically used in inhibitory network models. Re-doing simulations similar to Wang and Buzsáki (1996), they found that their coherent network oscillations exhibited higher frequencies and were more robust to heterogeneities. Since the modelling studies [Bartos et al., 2001, Bartos et al., 2002, Wang and Buzsáki, 1996] were performed using large (100-cell) networks along with the consideration of other issues (such as amount of connectivity and electrical coupling), it is difficult to determine the underlying mechanisms that give rise to the different network characteristics (frequency and coherence). However, as shown by White and colleagues (1998), using smaller (two-cell) networks is helpful in understanding larger network dynamics. Specifically, they identified two different ways in which coherence could be lost. This occurred in two different regimes, termed phasic and tonic, as identified by different values of the ratio of time constant and network period. Their

work shed light on why optimal synchronization at particular frequencies might be obtained in the larger networks. However, White et al.'s (1998) studies were restricted to regions of mild heterogeneity ($< 5\%$ difference in intrinsic frequencies).

In this paper, we explore how the amount of input heterogeneity to two-cell inhibitory networks affects their dynamics. We find that heterogeneity can be used to determine an optimal set of model parameters for coherent rhythms. Further, we show that coherence properties are preserved in larger (10-cell) networks suggesting that a strategy of "embedding" small network dynamics in larger networks might be a useful way to understand the contribution of biophysically-derived parameters to population dynamics in large networks.

2 Model and methods

We use a single compartment model developed by Wang and Buzsáki (WB) (1996) to represent the intrinsic properties of a hippocampal interneuron cell. The equations for each cell are given by:

$$\begin{aligned} C\frac{dV}{dt} &= I_{app} - g_{Na}m_\infty^3 h(V - V_{Na}) - g_K n^4(V - V_K) \\ &\quad -g_L(V - V_L) \qquad (1) \\ \frac{dh}{dt} &= \phi(\alpha_h(V)(1-h) - \beta_h(V)h) \qquad (2) \\ \frac{dn}{dt} &= \phi(\alpha_n(V)(1-n) - \beta_n(V)n) \qquad (3) \end{aligned}$$

where V is the cell membrane voltage in mV, h is the inactivation of the sodium current, n is the activation of the potassium current, and t is time in ms. m_∞ is the steady state activation of the sodium current and is given by: $m_\infty = \alpha_m/(\alpha_m + \beta_m)$, where $\alpha_m(V) = -0.1(V + 35)/(\exp(-0.1(V+35))-1)$, $\beta_m(V) = 4\exp(-(V+60)/18)$. $\alpha_h(V) = 0.07\exp(-(V+58)/20)$, $\beta_h(V) = 1/(\exp(-0.1(V+28))+1)$, $\alpha_n(V) = -0.01\exp(-(V+34)/\exp(-0.1(V+34))-1)$, $\beta_n(V) = 0.125\exp(-(V+44)/80)$, $\phi = 5$. Maximal sodium, g_{Na}, potassium, g_K, and leak, g_L, conductances are: 35, 9 and 0.1 mS/cm^2 respectively. Reversal potentials, V_{Na}, V_K, V_L, are 55, -90 and -65 mV respectively, and the capacitance, C, is 1 μF/cm^2.

We consider neuronal networks formed due to coupling via inhibitory synapses that are described by first order kinetics. The inhibitory synaptic current, I_{syn}, which would be added to the current balance equation of the postsynaptic cell, is given by:

$$I_{syn} = g_{syn}s(V - V_{syn}) \qquad (4)$$

where

$$\begin{aligned} \frac{ds}{dt} &= \alpha T(V_{pre})(1-s) - s/\tau_{syn} \qquad (5) \\ T(V_{pre}) &= \frac{1}{1+\exp(-V_{pre}/2)} \qquad (6) \end{aligned}$$

and V_{pre} is the voltage of the presynaptic cell, g_{syn} is the maximal inhibitory synaptic conductance, $V_{syn} = -75$ mV is the synaptic reversal potential, $\alpha = 6.25$ ms^{-1} is the rate constant of the synaptic activation taken from [Bartos et al., 2001], and τ_{syn} is the synaptic decay time constant. τ_{syn} values as low as 1 ms were measured between hippocampal basket cells [Bartos et al., 2002], and so we explore a τ_{syn} range of 1 to 10 ms in our simulations, with a 1 ms resolution. g_{syn} values of 0.05, 0.15, 0.25, 0.35 and 0.5 mS/cm^2 are used since they encompass physiological values as measured in [Bartos et al., 2001, Bartos et al., 2002].

I_{app} represents the applied or external drive to the cell, and we use this parameter to introduce heterogeneity into the system. We consider two-cell networks that are reciprocally coupled and ten-cell all-to-all coupled networks.

For the two-cell networks, the external drive to cell 1 or 2 is:

$$\begin{aligned} I_{app,1} &= I_\mu - \epsilon \quad \text{or} \\ I_{app,2} &= I_\mu + \epsilon \end{aligned}$$

respectively, so that their external drives differ by 2ϵ. We define the percent heterogeneity, %Het, as:

$$\%\text{Het} = \frac{(I.F. \text{ at } I_{app,2}) - (I.F. \text{ at } I_{app,1})}{I.F. \text{ at } I_{app,2}} \times 100\% \tag{7}$$

where $I.F.$ is the intrinsic frequency of the isolated cell. I_μ values of 1, 2 and 3 μA/cm^2 are explored systematically, as well as I_μ values of 4 μA/cm^2 using g_{syn} values of 0.25 mS/cm^2. %Het values exceeding 30% are examined systematically in simulations to determine the robustness of coherent oscillations. In summary, parametric variations of $g_{syn}, \tau_{syn}, I_\mu$ and ϵ are examined.

For the ten-cell networks, the I_{app}'s are randomly chosen from a uniform distribution in the interval [$-$%Het, $+$%Het]. All-to-all coupled networks are simulated and g_{syn} values are normalized so that each presynaptic cell "delivers" a maximal inhibition of $g_{syn}/9$.
A measure based on [White et al., 1998] is used to determine network "coherence" or the level of synchrony present in the ten-cell networks. This measure approximates the amount of overlap that exists between two spiking cells where the amount of overlap used is 20% of the period of the faster firing cell. Briefly, the spike trains of each pair of neurons are approximated by a series of square pulses of unit height and fixed width of 20% of the period of the faster firing cell. The shared area of the square pulses from each train that overlap in time is calculated for a given duration. This is equivalent to taking the cross correlation at zero time lag. The average between all pairs is taken, and the last 2 seconds of the ten-cell simulations (which were 5 seconds in total) were used as the duration to calculate the coherence measures presented in the paper. Gaussian noise is included in some of the ten-cell simulations by adding it to the current balance equation of each cell (i.e., equation (1)). Zero mean and standard deviations (SDs) from half to twice the amount of heterogeneity in the system is used.

Network simulations are performed using a modified version of our in-house software, NNET [Murray, 2004, Skinner and Liu, 2003], which integrates the system of differen-

tial equations using CVODE [Cohen and Hindmarsh, 1996]. Unless otherwise stated, initial conditions (ICs) for the two-cell network simulations are: $V_1 = -58.7249$, $V_2 = -55.0456$, $h_1 = h_2 = 0.9379$, $n_1 = n_2 = 0.1224$, $s_1 = s_2 = 0.1386$. In some cases these values were varied, but this was not done systematically.

A dynamical systems approach for studying nonlinear ordinary differential equations, such as equations (1)-(3), involves bifurcation analyses, in which the dependence of solutions to the differential equations on various parameters is examined. Solutions include steady states and oscillations. A well-known feature of nonlinear systems is its ability to express multiple stable solutions, i.e., multistability. For a fixed set of parameters, one can determine equilibrium points for the system. For example, V values that do not change with time, $dV/dt = 0$ (see equation (1)) and so on. It is the stability of these equilibrium points that determines the particular solution(s) that the system expresses (steady states, oscillations etc.). A dynamical system is said to undergo a bifurcation if the qualitative dynamics of the system are different above and below a particular value of a parameter. The value where the change occurs is called a bifurcation value. For example, the WB model ([Wang and Buzsáki, 1996]) has an I_{app} bifurcation value close to 0.2 μA/cm^2 in that below this I_{app} value, the model system expresses a steady state voltage output, and above this value, the model system produces an oscillatory output, i.e., repetitive firing. Bifurcations are considered local or global depending on details regarding the number of equilibrium points and their stability characteristics. Common local bifurcations are Hopf bifurcations and saddle-node bifurcations, and common global ones are homoclinic bifurcations and saddle node of limit cycles bifurcations. Knowing the specific type of bifurcation that a system expresses as particular parameters are varied can allow one to predict the presence of multistable patterns. For example, a subcritical Hopf bifurcation arising in a bifurcation analysis using a particular parameter means that bistability exists for a range of values of the particular parameter. So, for a given parameter value in that range, the system expresses two stable patterns, say oscillations and steady states. A bifurcation diagram is a way to illustrate the stability of equilibirum points and periodic solutions as a particular parameter is varied (e.g., see Figure 6). Since it is hardly ever possible to perform these calculations analytically, numerical techniques must be employed. A numerical continuation refers to using numerical approaches to find equilibrium points and periodic solutions, and to examine how their stability changes as parameters are varied. Although challenging to set up and run, numerical continuations have the advantage over numerical simulations of easily finding multistability and finding highly accurate bifurcation values. Numerical solutions from simulations can only produce stable solutions. If multistability is present, the solution produced depends on the initial conditions.

We perform several bifurcation analyses using AUTO [Doedel, 1981] in the XPPAUT software package [Ermentrout, 2002]. Depending on the particular set of parameters, step sizes are adjusted to allow continuation of solutions along the various branches. However, the maximum stepsize used to obtain the results shown in Tables 3 and 4 is 0.001 (thus determining the resolution).

3 Results

3.1 Dynamic patterns in two-cell heterogeneous networks

In homogeneous, two-cell inhibitory networks, in-phase (synchronous) and anti-phase oscillations are possible depending on the particular parameters in operation [Lewis and Rinzel, 2003, Skinner et al., 1994, Wang and Rinzel, 1992]. When mild heterogeneity is introduced into the two-cell system, harmonic locking and asynchronous states are also obtained [White et al., 1998]. For the ranges of parameters explored (see Methods), we obtained five distinct patterns in our two-cell network simulations. These observed patterns are: (i) near-synchronous, (ii) near-antiphase, (iii) varied phase-locking with small phase lags (i.e., one-to-one, but period varies, and phase lags are $< 10\%$), (iv) suppressed states, and (v) harmonic locking. Examples of each of these are shown in Figure 1A-E. In addition, we obtained dynamic states that did not express any clear pattern, referred to as asynchronous behaviour. We considered the pattern to be asynchronous if we did not observe any of patterns (i)-(v) after at least one second of simulation time when transients should no longer be apparent (given the time constants involved in the model). We examined at least 25 spikes after transients before concluding that there was no clear pattern. An example is illustrated in Figure 1F. Multistable patterns were uncovered in some parameter ranges when different initial conditions were explored. We also obtained patterns that are mixtures of the above patterns. Since these mixture variants did not occur in any obvious fashion, we did not examine them further here. Assuming that closely aligned firing of cells in inhibitory networks are necessary for generating population rhythms, one expects that patterns (i) (Figure 1A) and (iii) (Figure 1C) are the most relevant.

In Figure 2, we show two examples of the occurrence of these different patterns as τ_{syn} and %Het are varied for given g_{syn} and I_μ values. As g_{syn} was increased, the amount of the %Het$-\tau_{syn}$ plane that is represented by suppressed states increased. For smaller g_{syn} values, harmonic locking states dominated the plane. We also found that for smaller I_μ values more suppressed states occurred over the %Het$-\tau_{syn}$ plane (not shown). The expression of suppressed states in the plane can be somewhat understood by results obtained in previous modelling studies by [White et al., 1998]. Although they did not specifically discuss how their network dynamics changed with variations in the amount of heterogeneity in the system, they did find that there are two different mechanisms by which networks could lose coherence in the presence of mild heterogeneity ($< 5\%$ difference in intrinsic frequencies). For one of the mechanisms, in their so-called *phasic* regime, τ_{syn}/T has smaller values relative to the tonic regime (where T refers to the network period). Coherence occurs in this regime, and is lost via suppressed states for smaller I_{app} and larger g_{syn} values (see Figure 2, bottom).

3.2 Robust network oscillations

Since we are assuming that closely aligned firing of the cells in the inhibitory networks are important for generating population rhythms, we define the robustness of a two-cell network as its ability to express near-synchronous network oscillations (i.e., "coherence") in

the face of heterogeneity of external inputs received (i.e., $\epsilon \neq 0$). A stronger robustness means that the network can express coherence for larger amounts of heterogeneity. In Figure 2 (top), we see that the robustness of the two-cell system increased as τ_{syn} was increased up to just under 7%Het for $\tau_{syn} = 10$ ms. We can consider a measure of the robustness of an inhibitory network system as the maximal %Het expressed for a given set of parameters. Therefore, in Figure 2 (top), the robustness or maximal %Het for $\tau_{syn} = 1$ is 4%. Interestingly, our simulations indicate that there might be an optimal set of parameters that maximizes the network robustness. In particular, Figure 2 (bottom) shows that for $\tau_{syn} = 5 - 6$ ms (with I_μ=3 μA/cm^2, g_{syn}=0.25 mS/cm^2), the system still expresses near-synchronous oscillations in the face of more than 11%Het – for larger and smaller values of τ_{syn}, the robustness is weaker.

In Table 1, we show parameter sets ($I_\mu, \tau_{syn}, g_{syn}$) for which robust oscillations were obtained in our simulations. We only list cases for which the robustness or maximal %Het exceeded 7%, and this maximal %Het for each parameter set is shown. In addition, network frequency and phase information is indicated. For all the cases shown in Table 1, the network pattern at the maximal %Het is the near-synchronous described pattern (i) (see Figure 1A for illustration). With heterogeneity beyond this maximal %Het, harmonic locking or suppressed states occurred, and asynchronous states (as defined above) sometimes preceded the suppressed states as the heterogeneity was increased. For most of the parameter sets, %Het values less than the maximal %Het shown in Table 1 also resulted in near-synchronous oscillations. However, near-antiphase, varied phase-locking and asynchronous patterns sometimes occurred at lower %Het values (see Figure 3), as well as bistable patterns (see Figure 4). There would be an additional three cases to include in Table 1 from our simulations if we also encompassed maximally robust oscillations with varied phase-locking patterns (iii) (see Figure 1B for illustration). In those cases, a further increase in heterogeneity gave way to suppressed behaviours at larger %Het values. These observations are naturally limited by the resolution of the simulations performed (see Methods).

Not surprisingly, the phase lag in the near-synchronous states increased as the heterogeneity was increased (not shown). This is mainly responsible for the observed decrease in network frequency as the heterogeneity increases for a given parameter set. That is, with more heterogeneity, the closeness of the aligned spikes in the two cells (when it occurs) increases, and the network period is larger. As expected (observed in previous modelling studies of [Wang and Rinzel, 1992, White et al., 1998]), the network frequency increased with decreasing τ_{syn}. Any two rows (with different τ_{syn}) in Table 1 where the %Het is the same can be compared to see that this is the case.

Since it was found that τ_{syn}/T values separated tonic and phasic regimes (i.e., in reference to different ways in which coherence is lost [White et al., 1998]), we also calculated τ_{syn}/T for our network oscillations. This is shown in Table 1 for the robust oscillations with $>$ 7%Het. We found τ_{syn}/T to have "small" values in accordance with [White et al., 1998] who found that τ_{syn}/T was smaller (< 1, for their cellular model) for the phasic (as opposed to the tonic, > 2) regime where coherence occurs. Together with the observation from

our simulations that there seems to be an optimal set of parameters $(I_\mu, g_{syn}, \tau_{syn})$ that maximizes the network robustness, one can define a window of τ_{syn}/T values for which maximal robustness occurs.

As derived from several simulations, a non-monotonic dependence of robustness on each of the parameters g_{syn}, I_μ and τ_{syn} occurs. This is shown in Figure 5. The exact values for maximal %Het and τ_{syn}/T of Figure 5 are given by the boldfaced values in Table 1 for maximal %Het values or robustness measures exceeding 7%. These data indicate that it might be possible to determine a set of model parameters that give rise to maximally robust network oscillations. However, our simulations also show that the dynamics in these two-cell networks express much complexity. For example, Figure 4 shows an example of bistability, and Figure 3 shows how several dynamic patterns can be expressed for small changes in heterogeneity. The patterns shown in Figure 3 were obtained for a chosen set of initial conditions (see Methods). However, given the nonlinearity of the system, other stable patterns likely exist for these same parameter values. For the set of initial conditions used, Figure 3 shows that increasing the heterogeneity can be helpful in bringing about "coherence" or near-synchronous solutions.

3.3 Bifurcation analysis of two-cell heterogeneous networks

To establish the validity of our simulation observations regarding the existence of maximal robustness, we embarked on a bifurcation analysis (see description in Methods). Our observations might depend on the nonlinear relationship between I_{app} and the intrinsic frequency, but it is not obvious that a non-monotonic dependence of robustness on parameters as shown in Figure 5 should exist. We performed a series of numerical continuations of the two-cell heterogeneous network system. Our simulations led us to focus mainly on $g_{syn} = 0.15, 0.25, 0.5$ mS/cm^2 values as where the most robust network oscillations were present (see Table 1). Continuations using either I_μ or ϵ as the bifurcation parameter (see Tables 2 and 3) for a range of τ_{syn} values were done. We were able to determine the existence and stability of both the equilibria and periodic solutions of the system as the I_μ or ϵ parameter was varied while the other parameters remained fixed. This allowed us to obtain the precise dependence of coherence in the model network system on variations in specific parameter values.

In Figure 6A we show a typical bifurcation diagram with I_μ as the bifurcation parameter. Recall that a bifurcation diagram is an illustration of the dependence on a particular parameter of the stability of equilibrium points and periodic solutions (see further description in Methods). The stable equilibria are represented by thin solid lines and unstable equilibria by thin dashed lines. Periodic solutions are represented by lines showing their maximum amplitude at each parameter value. Stable periodic solutions are denoted by thick solid lines whereas unstable periodic solutions are given by thick dashed lines. We followed three distinct sets of oscillations: two suppression oscillations (either cell 1 suppressing cell 2 or vice versa) which emanated from two Hopf bifurcations (marked by an open box in Figure 6A), and a near-synchronous oscillation. In terms of stability, for large I_μ (> 25 μA/cm^2)

there was only a stable steady state solution, as illustrated by the thin solid line. This means that the cells remained at a steady voltage value (e.g., at $I_\mu = 30$, this value for cell 1 is about -30 mV, see Figure 6A). For mid range values of I_μ ($10 - 25$ μA/cm^2), only a near-synchronous oscillation was stable. For I_μ values explored in the simulations above (i.e., 1 - 4 μA/cm^2), the two suppression oscillations and the near-synchronous oscillation were sometimes all stable. This can be seen in Figure 6B which is an expansion of the relevant region of the bifurcation diagram of Figure 6A. For small I_μ, the suppression oscillations were lost via a homoclinic bifurcation and the near-synchronous oscillations lost stability via a period doubling bifurcation (marked by an open circle in Figure 6A,B) and then disappeared either in a homoclinic bifurcation or a saddle node of limit cycles bifurcation. For large values of τ_{syn} (as in Figure 6A,B), the system went to a suppression oscillation when the near-synchronous oscillations lost stability. For smaller values of τ_{syn}, the region of stability of the suppression oscillations decreased and when the near-synchronous oscillations lost stability the system exhibited either asynchronous or harmonically-locked oscillations. We summarize the results from several numerical continuations in Table 2. All these particular continuations were performed using $\epsilon = 0.05$ μA/cm^2. Note that these continuations were performed with I_μ as the bifurcation parameter, and so the other parameters (including ϵ) were fixed at particular values as indicated in Table 2. For each case, the minimum I_μ for which near-synchronous behaviour is present is indicated (e.g., see Figure 6B example). This I_μ together with ϵ determines the %Het for the system and this is also shown in Table 2. Note that decreasing I_μ corresponds to increasing the %Het in the system because of the nonlinear relationship between I_{app} and the intrinsic frequency of the isolated WB model cell [Wang and Buzsáki, 1996]. For this choice of ϵ and with $g_{syn} = 0.25$ mS/cm^2 we can see that as τ_{syn} decreases, one obtains a %Het that increases until it reaches a maximum and then decreases. In other words, for a fixed difference in external input (as given by ϵ), the minimal required amount of external drive to give rise to near-synchronous oscillations can both increase and decrease with increasing τ_{syn}.

Near-synchronous and suppression solutions were found and followed in our numerical continuation studies. Other solutions such as varied phase-locking and antiphase oscillations are present in various parameter regimes (as shown from simulation studies), but were not systematically followed in the studies performed here. A typical bifurcation diagram with ϵ as the bifurcation parameter is shown in Figure 6C. As ϵ (and hence %Het) was increased, the stable near-synchronous oscillations were lost in one of two ways. They either ceased to exist via a saddle node of limit cycles (as shown in Figure 6C) or they lost stability in a period doubling bifurcation before the saddle node of limit cycles. For large τ_{syn}, when the stable near-synchronous oscillations were lost, the system exhibited suppression oscillations. As τ_{syn} was decreased, the region of existence of the suppression oscillations was diminished. For τ_{syn} small enough (e.g., see Figure 6C), this region no longer overlapped with the region of stability of the near-synchronous oscillations. The system exhibited either harmonically-locked or asynchronous oscillations when the stable near-synchronous oscillations were lost, and suppression oscillations at larger values of ϵ or %Het as shown in Figure 6C. In Table 3, we indicate the largest value of ϵ for which stable near-synchronous oscillations exist for

each given set of parameter values, as determined from several numerical continuations. As τ_{syn} decreases, it is clear that a maximal %Het exists. Specifically, for $g_{syn} = 0.25$ mS/cm^2, $I_\mu = 3$ μA/cm^2, and $\tau_{syn} = 5$ ms, there is a maximal %Het of 12.5%. We conclude that the non-monotonic dependence of robustness on different parameters as observed in the simulations (see Figure 5) is a well-defined phenomenon.

3.4 From two to ten-cell heterogeneous networks

Now that we have established that there exists a set of parameters which give rise to maximally robust oscillations, we would like to determine whether coherence properties observed in the two-cell networks are borne out in larger networks. That is, are the parameter regimes for robust oscillations in two-cell networks similar to parameter regimes in larger networks? Consider the simplified view that if one uniformly distributes the amount of heterogeneity up to a maximal amount between a set of cells, then the possible patterns that the network expresses would include those observed in the two-cell network for the given heterogeneity. Therefore, parameter values that give rise to coherent oscillations in larger (> two-cell) networks could be predicted from what is known about coherent oscillations in the two-cell networks.

In Table 4 we show coherence measure values obtained from several ten-cell network simulations. For the top part of Table 4, the simulations used parameter values of $g_{syn} = 0.25$ mS/cm^2, I_μ=3 μA/cm^2, and $\tau_{syn} = 1$ or 5 ms. Using these same parameters, two-cell network simulations produced coherent oscillations up to 5.8%Het with $\tau_{syn} = 1$ ms, and up to 11.4%Het with $\tau_{syn} = 5$ ms. Furthermore, near-synchronous solutions were obtained when smaller %Het values were used in the two-cell simulations (using initial conditions given in the Methods). With τ_{syn}=1 ms, the ten-cell network simulations produced coherent oscillations with 3%Het, but not with 8%Het as given by their coherence values shown in Table 4. When τ_{syn} was increased to 5 ms, the ten-cell networks with 3%Het were still very coherent, but now the ten-cell networks with 8%Het were also coherent. That is, using 8%Het, the coherence measure value obtained with $\tau_{syn} = 5$ ms is larger than with $\tau_{syn} = 1$ ms. However, as with $\tau_{syn} = 1$ ms, the coherence value obtained with 8%Het is smaller than with 3%Het, but to a lesser extent. Given that the two-cell networks show "coherence" up to 5.8%Het with $\tau_{syn} = 1$, but up to 11.4%Het with $\tau_{syn} = 5$, it would appear that the coherence properties of two-cell heterogeneous networks are "preserved" in the larger networks. The ten-cell simulations were re-done with the addition of noise (see Methods). We used Gaussian noise with standard deviations (SDs) that were half of, equal to, and twice that of the level of heterogeneity in the system. In all cases, the difference in coherence, as "predicted" from the two-cell simulations was maintained (see Table 4).

As shown in Figures 4 and 6B, bistable patterns can occur in the two-cell heterogeneous network system. The bistable pattern illustrated in Figure 4 was obtained using parameters of $g_{syn} = 0.25$ mS/cm^2, I_μ=1 μA/cm^2, and $\tau_{syn} = 1$ ms. The initial conditions were such that the initial voltages were either: (i) different by about 4 mV, as given in the Methods, or (ii) the same for the two cells, $V_1 = V_2 = -59.5567$. The initial values for the

other variables (h, n, s) of each model cell were the same for the two cases and are given in the Methods (see Figure 4 legend). With increasing heterogeneity, for the first case of initial conditions, we obtained near-antiphase patterns (up to 4%Het), then varied phase-locking, and then near-synchronous patterns up to a 8%Het. Harmonic locking patterns arose with further increases in heterogeneity. For the second case of initial conditions, we obtained varied phase-locking and then near-synchronous patterns with increasing heterogeneity up to 8%Het, and then harmonic locking as in the first case of initial conditions. (The particular patterns for the case of 4%Het are shown in Figure 4.) Using these parameter values in a ten-cell network configuration, we find again that the two-cell dynamics "predict" the coherence properties of the ten-cell networks. Consider two different initial conditions for the ten-cell networks that are derived from the two cases of initial conditions for the two-cell networks. They are either (i) the initial voltages for the ten cells were different (but within 5 mV of each other), or (ii) the initial voltages were all the same value. As in the two-cell network simulations, the initial values for the other variables (h, n, s) of each model cell were the same for the two cases. We will refer to the first and second case of initial conditions (ICs) for the ten-cell networks as ICs_A and ICs_B respectively, and they are given with Table 4. The bottom part of Table 4 provides coherence values obtained from ten-cell network simulations with ICs_A and ICs_B. Since the heterogeneity is spread uniformly among the ten cells, and if the dynamic behaviours seen in the two-cell networks occur in the larger networks, then one might expect to see larger coherence values with ICs_B than with ICs_A. We found this to be the case with 5%Het. At and below this level of heterogeneity, the two-cell network dynamics mostly included near-antiphase (i.e., non-coherent) patterns with initial conditions given by the first case, and so the vast difference in coherence values observed in the ten-cell simulations is supportive of the predictive nature of the two-cell network dynamics for larger networks. However, when we increased the heterogeneity further to 8%Het in the ten-cell simulations, this large difference in coherence values using the two different ICs was no longer apparent. Since at and below this amount of heterogeneity, both sets of ICs now mostly involve near-synchronous patterns in two-cell networks, this does not negate the predictive aspect of the two-cell dynamics for larger (ten-cell) network coherence. It suggests that non-coherent patterns (such as antiphase) need to dominate the two-cell network dynamics (at the particular level of heterogeneity) to manifest their effect in larger networks. Interestingly, when noise is added to the simulations (e.g., see the last column of Table 4 which is boldfaced), the dependence on the exact level of heterogeneity is removed. For both 5%Het and 8%Het, the ten-cell networks have a much lower coherence value when ICs_A are used as near-antiphase patterns occur in the two-cell networks using the first case of initial conditions described above. The above results support the possibility that coherence properties in larger networks can be predicted from dynamic patterns obtained in two-cell networks. However, one should caution that such observations would depend in some fashion on the particular choices of initial conditions, noise levels and the dynamic constraints on different stable patterns expressed by nonlinear systems, as has been examined for homogeneous inhibitory networks [Golomb and Rinzel, 1994].

4 Discussion

Our results show that the robustness of network oscillations has a non-monotonic dependence on synaptic time constant, synaptic conductance and mean external drive. This suggests that there is an optimal set of parameters for which robust "coherent" network oscillations occur. One can consider determining this set of parameters which then defines the network output for the particular cellular model being used. Our bifurcation and simulation studies using a WB cellular model show that an optimal set of parameters occurs when $g_{syn} = 0.25$ mS/cm^2, $I_\mu = 3\,\mu$A/cm^2, and $\tau_{syn} = 5$ ms, where robust network oscillations with $> 12\%$Het occur (see Figure 2 and Table 3). With these values, the two-cell heterogeneous network exhibits oscillations of about 90Hz frequency and with about a 10% phase lag between the two cells. Although a direct comparison with the 100-cell network simulation results of [Bartos et al., 2001, Bartos et al., 2002, Wang and Buzsáki, 1996] cannot be made, our results go some way in explaining the more robust and higher frequency oscillations observed by Bartos et al. (2001, 2002) in their simulations as compared to simulations performed by Wang and Buzsáki (1996). In addition, our simulations show that two-cell coherence properties are maintained in larger ten-cell networks. Together with other studies by White et al. (1998) showing similar qualitative behaviours in 2, 10 and 100-cell networks, our work suggests that using the amount of heterogeneity (i.e., ϵ) as a parameter in (two-cell) network studies allows the determination of optimal parameter values which in turn are predictive of coherent regimes in larger networks.

4.1 Biophysical detail and external input

In developing mathematical models of neuronal networks that include some sort of biophysical characteristics, it is useful to have constraints on a chosen model's parameters. Questions regarding model detail naturally arise: how much and what? For inhibitory network models targeted towards hippocampal cortex, there are network model explorations using cellular inhibitory models that are: detailed multi-compartment representations (e.g., [Maex and De Schutter, 2003, Traub and Bibbig, 2000]), single compartment representations (e.g., [Baker et al., 2002, Jalil et al., 2004, Tiesinga and José, 2000, Wang and Buzsáki, 1996, Wang, 2002, White et al., 1998]), or simpler integrate-and-fire units (e.g., [Brunel and Wang, 2003, Neltner et al., 2000]). To a large extent, the amount of biological detail that makes sense to include in a neuronal model depends on the question being asked. While analyzing and determining underlying cellular mechanisms in network models give rise to constraints on some parameters for given dynamic outputs, one is still often faced with few or no constraints on other model parameters. A problem faced by all modellers is how best to *both* incorporate biophysical detail and do mathematical analyses to understand and predict the model output. The intrinsic cellular properties of a model always make a difference to the network output, but it may not be a critical difference. While an examination of time constant values and active voltage ranges for particular ion currents is suggestive of the importance of particular intrinsic properties, this is a qualitative estimation that is subject to non-intuitive, nonlinear outcomes. We suggest that our criterion of

maximal heterogeneity could be used as a basis for evaluating how much of a "difference" various intrinsic details make to network coherence. That is, would the optimal $g_{syn}, I_\mu, \tau_{syn}$ values change with, say, using three (rather than two) types of potassium currents?

A critical parameter in network models is the external or applied current, I_{app}. However, there is no well-defined way to measure this parameter value as it represents the summation of synaptic and background current (noise and heterogeneities) in the dendritic tree, which in turn depends on the integration properties of the particular cell and the network in which it resides. Depending on whether the individual cell model includes a dendritic component and on what network size is being considered, the input could be described by a tonic current or Poisson statistics with or without noise, heterogeneities and correlations [Brunel and Wang, 2003, Destexhe et al., 2003, Maex and De Schutter, 2003, McMillen and Kopell, 2003]. Interestingly, Maex and DeSchutter (2003) show that the difference between using tonic or afferent fiber input (Poisson statistics) is not important in extracting a resonant synchronization in their inhibitory networks. A modification of our suggestion above would be to determine the I_μ (i.e., I_{app}) value that gives the most robust oscillations for the given cellular model. In this way, the choice of I_{app} would be less arbitrary than simply using values that give rise to certain network frequencies.

4.2 Network modelling strategies and related works

The best strategy to use if one wants to understand network dynamics in which the biophysical details are not ignored is unclear. However, strategies for particular problems have been developed [Ermentrout and Chow, 2002]. For example, for problems involving long-distance synchronization, a mapping strategy was introduced by [Ermentrout and Kopell, 1998] in which the biophysical equations can be reduced to a one-dimensional map in terms of spike timings of different neurons. The subsequent map is then easily analyzed and its predictions verified with simulations (e.g., [Acker et al., 2003]). A geometric approach, in which several trajectories (each corresponding to one cell) move around in a lower dimension phase space has been used to understand thalamic oscillations [Rubin and Terman, 2000]. Otherwise, one can test predictions from simpler (integrate-and-fire) models using more detailed biophysical models (e.g., see [Wilson et al., 2004]). A more general strategy using the theory of weakly coupled oscillators [Kuramoto, 1995] allows one to mathematically reduce the network system to a set of equations only involving phases. These equations are then straightforward to analyze. While this approach is powerful and has been used to analyze networks of coupled cells (e.g., [Chow, 1998, Lewis and Rinzel, 2003, Neltner et al., 2000]), it is limited to neuronal units that exhibit stable limit cycles and which have sufficiently weak coupling.

The ability to continue solutions when doing bifurcation analyses is constrained by the complexity of the set of nonlinear equations. As shown in our work here, this is feasible using two-cell networks, but is clearly impractical for large networks. However, since it seems that the coherent properties in two-cell networks can be preserved in larger networks, it might be a useful small-to-large network modelling strategy to determine optimal external

input and/or intrinsic biophysical parameters from two-cell network analyses via the maximal heterogeneity criteria suggested above. Depending on what experimental data is available, it might also be reasonable to determine some optimal synaptic parameters in this way. Then, in performing larger network simulations, one would already have intuition from the two-cell network dynamics so that it may be possible to fundamentally understand any observed changes in coherence patterns of the large networks. In addition, one could attempt to mathematically reduce the intrinsic cell model with its optimal parameters to subsequently use in larger network simulations.

Our results are in accordance with other modelling studies of heterogeneous, inhibitory networks. In the 100-cell simulation studies by Bartos et al. (2001, 2002) and Wang and Buzsáki (1996), a Gaussian distribution of heterogeneities was used and different amounts were explored for specific parameter values (e.g., see Figure 5 in [Wang and Buzsáki, 1996]). Neltner et al. (2000) defined robustness of synchrony as the critical disorder at which the asynchronous state becomes linearly stable. With this definition, they obtained a maximal robustness using WB neurons when synaptic conductance was varied, for a given time constant and mean frequency. In another modelling study, Tiesinga and José (2000) suggest that stochastic weak synchronization (as opposed to strong synchronization), in which the particular cycle in which each cell fires is random, might underlie robust oscillations in inhibitory networks.

4.3 Basket cell networks in hippocampus

This study was partly motivated out of concern for how to constrain cellular models used in inhibitory networks. Developing models of individual interneurons in hippocampus that encompass the richness of their intrinsic properties is a major undertaking (e.g., [Saraga et al., 2003]). Furthermore, there is usually not enough experimental data for particular interneurons to warrant developing a very detailed model. However, if one then uses a simplified model, it is unclear how best to constrain the chosen parameters. Our study here suggests how optimal parameters might be determined. It is interesting to note that Bartos et al. (2002) found differences in synaptic time constants and peak synaptic conductances in DG, CA3 and CA1 regions of hippocampus in inhibitory basket cells. One could envisage using the particular τ_{syn} and g_{syn} values to select out an I_μ value via our maximal heterogeneity criterion. This I_μ value in turn would give rise to a certain network frequency. One might speculate that particular hippocampal regions are "tuned" to particular frequencies. Basket cell networks are also connected by gap junctions, which adds another layer of complexity [Freund, 2003, Fukuda and Kosaka, 2000]. This further emphasizes the importance of trying to understand local inhibitory circuits in the brain from the perspective of biophysical parameter values. Our work shows how this could be approached.

Acknowledgements: This work was supported by NSERC of Canada. F.K.S. is an MRC Scholar and a CFI Researcher.

References

[] Acker, C. D., Kopell, N., and White, J. A. (2003). Synchronization of strongly coupled excitatory neurons: Relating network behavior to biophysics. *J. Comput. Neurosci.*, 15:71–90.

[] Baker, P. M., Pennefather, P. S., Orser, B. A., and Skinner, F. K. (2002). Disruption of coherent oscillations in inhibitory networks with anesthetics: the role of $GABA_A$ receptor desensitization. *J. Neurophysiol.*, 88:2821–2833.

[] Bartos, M., Vida, I., Frotscher, M., Geiger, J. R. P., and Jonas, P. (2001). Rapid signaling at inhibitory synapses in a dentate gyrus interneuron network. *J. Neurosci.*, 21:2687–2698.

[] Bartos, M., Vida, I., Frotscher, M., Meyer, A., Monyer, H., Geiger, J. R. P., and Jonas, P. (2002). Fast synaptic inhibition promotes synchronized gamma oscillations in hippocampal interneuron networks. *Proc. Natl. Acad. Sci.*, 99(20):13222–13227.

[] Bragin, A., Jandó, G., Nádasdy, Z., Hetke, J., Wise, K., and Buzsáki, G. (1995). Gamma [40-100 Hz] oscillation in the hippocampus of the behaving rat. *J. Neurosci.*, 15:47–60.

[] Brunel, N. and Wang, X.-J. (2003). What determines the frequency of fast network oscillations with irregular neural discharges? I. Synaptic dynamics and excitation-inhibition balance. *J. Neurophysiol.*, 90(1):415–430.

[] Buzsáki, G. (2002). Theta oscillations in the hippocampus. *Neuron*, 33:325–340.

[] Buzsáki, G. and Chrobak, J. (1995). Temporal structure in spatially organized neuronal ensembles: A role for interneuronal networks. *Curr. Opin. Neurobiol.*, 5:504–510.

[] Chow, C. C. (1998). Phase-locking in weakly heterogeneous neuronal networks. *Physica D*, 118:343–370.

[] Cohen, S. D. and Hindmarsh, A. C. (1996). CVODE, a stiff/nonstiff ODE solver in C. *Computers in Physics*, 10:138–143.

[] Destexhe, A., Rudolph, M., and Paré, D. (2003). The high-conductance state of neocortical neurons *in vivo*. *Nature Rev. Neurosci.*, 4:739–751.

[] Doedel, E. J. (1981). AUTO: A program for the automatic bifurcation analysis of autonomous systems. *Congr. Numer.*, 30:265–284.

[] Ermentrout, G. B. (2002). *Simulating, Analyzing, and Animating Dynamical Systems: A Guide to XPPAUT for Researchers and Students.* SIAM, Philadelphia, http://www.math.pitt.edu/∼bard/xpp/xpp.html.

[] Ermentrout, G. B. and Chow, C. C. (2002). Modeling neural oscillations. *Physiol. Behav.*, 77:629–633.

[] Ermentrout, G. B. and Kopell, N. (1998). Fine structure of neural spiking and synchronization in the presence of conduction delays. *Proc. Natl. Acad. Sci. USA*, 95:1259–1264.

[] Freund, T. F. (2003). Interneuron Diversity series: Rhythm and mood in perisomatic inhibition. *Trends Neurosci.*, 26(9):489–495.

[] Freund, T. F. and Buzsáki, G. (1996). Interneurons of the hippocampus. *Hippocampus*, 6:347–470.

[] Fukuda, T. and Kosaka, T. (2000). Gap junctions linking the dendritic network of GABAergic interneurons in the hippocampus. *J. Neurosci.*, 20:1519–1528.

[] Golomb, D. and Rinzel, J. (1994). Clustering in globally coupled inhibitory neurons. *Physica D*, 71:259–282.

[] Jalil, S., Grigull, J., and Skinner, F. K. (2004). Novel bursting patterns emerging from model inhibitory networks with synaptic depression. *J. Comput. Neurosci.*, 17(1):23–37.

[] Kuramoto, Y. (1995). Collective behavior of coupled oscillators. In Arbib, M., editor, *The Handbook of Brain Theory and Neural Networks*, pages 203–206. Cambridge MA: MIT Press.

[] Lewis, T. J. and Rinzel, J. (2003). Dynamics of spiking neurons connected by both inhibitory and electrical coupling. *J. Comput. Neurosci.*, 14(3):283–309.

[] Maex, R. and De Schutter, E. (2003). Resonant synchronization in heterogeneous networks of inhibitory neurons. *J. Neurosci.*, 23(33):10503–10514.

[] McBain, C. and Fisahn, A. (2001). Interneurons unbound. *Nature Rev. Neurosci.*, 2:11–23.

[] McMillen, D. and Kopell, N. (2003). Noise-stabililized long-distance synchronization in populations of model neurons. *J. Comput. Neurosci.*, 15:143 –157.

[] Murray, P. A. (2004). Capturing details of short-term synaptic plasticity in simple schemes. *Master's Thesis, University of Toronto.*

[] Neltner, L., Hansel, D., Mato, G., and Meunier, C. (2000). Synchrony in heterogeneous networks of spiking neurons. *Neural Comput.*, 12(7):1607–1641.

[] Rubin, J. and Terman, D. (2000). Geometric analysis of population rhythms in synaptically coupled neuronal networks. *Neural Comput.*, 12:597–645.

[] Saraga, F., Wu, C. P., Zhang, L., and Skinner, F. K. (2003). Active dendrites and spike propagation in multi-compartment models of oriens-lacunosum/moleculare hippocampal interneurons. *J. Physiol.*, 552.3:673–689.

[] Skinner, F. K., Kopell, N., and Marder, E. (1994). Mechanisms for oscillation and frequency control in reciprocally inhibitory model neural networks. *J. Comput. Neurosci.*, 1:69–87.

[] Skinner, F. K. and Liu, J. B. (2003). NNET: linking small and large-scale network models. *Neurocomputing*, 52-54:381–387.

[] Tiesinga, P. H. E. and José, J. V. (2000). Robust gamma oscillations in networks of inhibitory hippocampal interneurons. *Network: Comput. Neural Syst.*, 11:1–23.

[] Traub, R. D. and Bibbig, A. (2000). A model of high-frequency ripples in the hippocampus based on synaptic coupling plus axon-axon gap junctions between pyramidal neurons. *J. Neurosci.*, 20:2086–2093.

[] Traub, R. D., Jefferys, J. G. R., and Whittington, M. A. (1999). *Fast Oscillations in Cortical Circuits*. MIT Press, Cambridge, MA.

[] vanVreeswijk, C., Abbott, L. F., and Ermentrout, G. B. (1994). When inhibition not excitation synchronizes neural firing. *J. Comput. Neurosci.*, 1:313–321.

[] Wang, X.-J. (2002). Pacemaker neurons for the theta rhythm and their synchronization in the septohippocampal reciprocal loop. *J. Neurophysiol.*, 87(2):889–900.

[] Wang, X.-J. and Buzsáki, G. (1996). Gamma oscillation by synaptic inhibition in a hippocampal interneuronal network model. *J. Neurosci.*, 16:6402–6413.

[] Wang, X.-J. and Rinzel, J. (1992). Alternating and synchronous rhythms in reciprocally inhibitory model neurons. *Neural Comput.*, 4:84–97.

[] Wang, X.-J. and Rinzel, J. (1993). Spindle rhythmicity in the reticularis thalami nucleus: Synchronization among mutually inhibitory neurons. *Neurosci.*, 53:899–904.

[] White, J. A., Chow, C. C., Ritt, J., Soto-Treviño, C., and Kopell, N. (1998). Synchronization and oscillatory dynamics in heterogeneous, mutually inhibited neurons. *J. Comput. Neurosci.*, 5:5–16.

[] Whittington, M. A., Traub, R. D., and Jefferys, J. G. R. (1995). Synchronized oscillations in interneuron networks driven by metabotropic glutamate receptor activation. *Nature*, 373:612–615.

[] Wilson, C. J., Weyrick, A., Terman, D., Hallworth, N. E., and Bevan, M. D. (2004). A model of reverse spike frequency adaptation and repetitive firing of subthalamic nucleus neurons. *J. Neurophysiol.*, 91:1963–1980.

[] Wu, C., Shen, H., Luk, W. P., and Zhang, L. (2002). A fundamental oscillatory state of isolated rodent hippocampus. *J. Physiol.*, 540.2:509–527.

FIGURE LEGENDS

Figure 1:
Different Dynamic Patterns Observed in Heterogeneous Two-cell Networks.
(A) Near-synchronous pattern. Parameters are: $g_{syn} = 0.15$ mS/cm^2, $\tau_{syn} = 6$ ms, $I_{app,1} = 1.9\mu$A/cm^2, $I_{app,2} = 2.1\mu$A/cm^2 (7%Het).
(B) Near-antiphase pattern. Parameters are: $g_{syn} = 0.5$ mS/cm^2, $\tau_{syn} = 1$ ms, $I_{app,1} = 0.985\mu$A/cm^2, $I_{app,2} = 1.015\mu$A/cm^2 (2.4%Het).
(C) Varied phase-locking pattern. Parameters are: $g_{syn} = 0.25$ mS/cm^2, $\tau_{syn} = 3$ ms, $I_{app,1} = 1.86\mu$A/cm^2, $I_{app,2} = 2.14\mu$A/cm^2 (9.7%Het).
(D) Suppression pattern. Parameters are: $g_{syn} = 0.25$ mS/cm^2, $\tau_{syn} = 5$ ms, $I_{app,1} = 1.9\mu$A/cm^2, $I_{app,2} = 2.1\mu$A/cm^2 (7%Het).
(E) Harmonic locking pattern. Parameters are: $g_{syn} = 0.25$ mS/cm^2, $\tau_{syn} = 2$ ms, $I_{app,1} = 1.8\mu$A/cm^2, $I_{app,2} = 2.2\mu$A/cm^2 (13.6%Het).
(F) Asynchronous pattern. Parameters are: $g_{syn} = 0.35$ mS/cm^2, $\tau_{syn} = 3$ ms, $I_{app,1} = 1.9\mu$A/cm^2, $I_{app,2} = 2.1\mu$A/cm^2 (7%Het).

Figure 2:
Percent Heterogeneity–Decay Time Constant (%Het–τ_{syn}) Plane of Dynamic Patterns.
Two examples are shown with parameters $g_{syn} = 0.15$ mS/cm^2 (top), and $g_{syn} = 0.25$ mS/cm^2 (bottom), with $I_\mu = 3$ μA/cm^2.
Black regions refers to near-synchronous patterns, white regions to suppressed patterns, grey regions to harmonic locking patterns, grey checked regions to asynchronous patterns and grey lined regions to near-antiphase patterns.

Figure 3:
Illustration of Changing Patterns with Changing Percent Heterogeneity (%Het).
As %Het increases from top to bottom, the dynamic patterns shown are: near-antiphase (2.2%Het), varied phase-locking (4.3%Het), asynchronous (5%Het), near-synchronous (7%Het), harmonic locking (7.7%Het) and near-synchronous (8.4%Het). With further %Het increases (up to 31%), harmonic locking patterns are obtained (not shown). In addition, between the asynchronous and near-synchronous patterns, there is another varied phase-locking pattern (not shown). Parameters are: $g_{syn} = 0.35$ mS/cm^2, $I_\mu = 2\mu$A/cm^2, $\tau_{syn} = 1$ ms.

Figure 4:
Example of Bistability.
Both near-antiphase (top) and varied phase-locking (bottom) patterns exist with 4%Het. For the near-antiphase pattern, the set of initial conditions used is given in Methods; for the varied phase-locking pattern, the set of initial conditions used is $V_1 = V_2 = -59.5567$, and the other variables have initial values as given in Methods. Parameters are: $g_{syn} = 0.25$ mS/cm^2, $I_{app,1} = 0.975\mu$A/cm^2, $I_{app,2} = 1.025\mu$A/cm^2, ($I_\mu = 1\mu$A/cm^2), $\tau_{syn} = 1$ ms.

Figure 5:
Non-monotonic Dependence of Robustness.
Two-cell network simulations give rise to coherent oscillations whose robustness depends

non-monotonically on parameters: g_{syn} (in mS/cm^2), and I_μ=2 μA/cm^2, τ_{syn}=4 ms (left); τ_{syn} (in ms), and g_{syn}=0.25 mS/cm^2, I_μ=3 μA/cm^2 (middle); I_μ (in μA/cm^2), and g_{syn}=0.25 mS/cm^2, τ_{syn}=4 ms (right). For each plot, the solid squares refer to the maximal %Het (for which coherence occurs) as given by the left hand ordinate axis, and the solid circles refer to τ_{syn}/T values as given by the right hand ordinate axis. The maximal %Het values that exceed 7% can be seen in Table 1. The non-monotonic relationship can be seen clearly by the solid line joining the squares. The "window" of τ_{syn}/T values that encompass this maximal robustness can by seen by the dashed line joining the circles. Note that the range of values shown on the axes for the three plots are not the same.

Figure 6:
Bifurcation Diagrams Showing Different Branches and Stabilities.
Each diagram shows the maximum value of V_1 (in mV) for each value of the bifurcation parameter. Stable/unstable equilibria are denoted by thin solid/dashed lines; stable/unstable periodic solutions by thick solid/dashed lines. Hopf bifurcations are indicated by an open box, period doubling by an open circle. (A) I_μ (in μA/cm^2) is the bifurcation parameter; other parameters are $g_{syn} = 0.5$ mS/cm^2, $\epsilon = 0.05\mu$A/cm^2, $\tau_{syn} = 10$ ms. (B) shows a blow up of (A) for I_μ in the range of 0 – 5 μA/cm^2. Bistable patterns of near-synchrony and suppression are present beyond I_μ of ≈ 3, i.e., the open circle. (C) ϵ (in μA/cm^2) is the bifurcation parameter; other parameters are $g_{syn} = 0.25$ mS/cm^2, $I_\mu = 3\mu$A/cm^2, $\tau_{syn} = 5$ ms. Illustrations in (A,B) and in (C) refer to boldfaced values in Table 2 and in Table 3 respectively.

Table 1: *Robust Oscillations in Two-Cell Model Networks: Near-Synchronous Oscillatory Solutions with %Het > 7%*

Parameters (g_{syn}, I_μ)	τ_{syn} (ms)	Maximal %Het	Netw.Freq. (Hz)	%Phase Lag	τ_{syn}/T
(0.05,1)	8	7.1	48.9	12.0	0.39
(0.05,1)	9	7.1	47.9	11.4	0.43
(0.05,1)	10	7.1	47.0	11.2	0.47
(0.15,1)	2	8.0	55.1	4.6	0.11
(0.15,1)	3	10.9	51.1	5.1	0.15
(0.15,2)	3	8.0	86.3	9.3	0.26
(0.15,2)	**4**	**9.0**	**81.8**	**8.9**	**0.33**
(0.15,2)	5	9.0	77.9	8.4	0.39
(0.15,2)	6	10.4	72.6	10.3	0.44
(0.15,2)	7	10.4	69.7	10.0	0.49
(0.15,2)	8	10.4	66.8	9.8	0.53
(0.15,2)	9	10.4	64.0	9.8	0.58
(0.15,2)	10	10.4	61.8	9.8	0.62
(0.25,1)	1	8.0	57.3	2.6	0.06
(0.25,2)	2	9.7	88.7	5.5	0.18
(0.25,2)	3	9.0	81.4	4.4	0.24
(0.25,2)	**4**	**7.0**	**75.2**	**3.4**	**0.30**
(0.25,3)	2	8.3	116.5	8.4	0.23
(0.25,3)	**3**	**9.6**	**107.3**	**8.1**	**0.32**
(0.25,3)	**4**	**10.8**	**98.0**	**9.2**	**0.39**
(0.25,3)	**5**	**11.4**	**90.5**	**9.5**	**0.45**
(0.25,3)	6	11.4	85.9	9.2	0.52
(0.25,4)	3	7.4	133.4	8.9	0.40
(0.25,4)	**4**	**7.9**	**124.5**	**10.4**	**0.50**
(0.25,4)	5	7.9	117.8	10.6	0.59
(0.25,4)	6	7.9	112.0	11.1	0.67
(0.25,4)	7	7.9	106.7	11.7	0.75
(0.25,4)	8	7.9	101.8	12.5	0.81
(0.25,4)	9	7.4	99.1	11.5	0.89
(0.25,4)	10	7.4	95.7	11.9	0.96
(0.35,1)	1	10.9	56.7	2.4	0.06
(0.35,2)	1	8.4	95.8	2.9	0.10
(0.35,2)	2	9.0	86.1	3.1	0.17
(0.35,3)	1	7.5	127.3	3.8	0.13
(0.35,3)	2	10.8	112.1	5.9	0.22
(0.35,3)	4	7.1	93.7	3.7	0.37
(0.5,3)	1	10.0	124.4	3.7	0.12

Table 2: *I_μ Bifurcation Parameter Results*

Parameters (g_{syn}, ϵ)	τ_{syn} (ms)	Min I_μ for NS	%Het (Min I_μ, ϵ)
(0.15,0.05)	5	0.526	15.967
(0.15,0.05)	2.5	0.799	10.656
(0.15,0.05)	1.4	1.212	5.981
(0.15,0.05)	1	1.558	5.354
(0.25,0.05)	10	2.180	3.461
(0.25,0.05)	6.7	1.901	3.722
(0.25,0.05)	5.7	1.808	3.714
(0.25,0.05)	5	1.743	5.108
(0.25,0.05)	3.3	1.683	5.222
(0.25,0.05)	2.5	1.755	3.888
(0.25,0.05)	2	1.749	3.818
(0.25,0.05)	1	0.937	9.925
(0.5,0.05)	**10**	**3.048**	**2.015**
(0.5,0.05)	7.1	2.513	3.266
(0.5,0.05)	6.7	2.436	3.298
(0.5,0.05)	5	2.338	3.378

Note: NS = near-synchronous oscillations. Bifurcation diagrams referring to bold-faced values are shown in Figure 6A,B.

Table 3: *ϵ Bifurcation Parameter Results*

Parameters (g_{syn}, I_μ)	τ_{syn} (ms)	Max ϵ for NS	Max %Het (I_μ, Max ϵ)
(0.15,2)	5	0.146	10.386
(0.15,2)	2.5	0.109	7.076
(0.15,2)	1.4	0.075	4.732
(0.15,2)	1	0.062	4.757
(0.25,3)	10	0.136	5.971
(0.25,3)	6.7	0.192	7.873
(0.25,3)	5.7	0.273	11.568
(0.25,3)	**5**	**0.267**	**12.491**
(0.25,3)	3.3	0.240	10.677
(0.25,3)	2.5	0.213	8.833
(0.25,3)	2	0.190	8.816
(0.25,3)	1	0.134	5.957
(0.5,5)	10	0.111	2.729
(0.5,5)	5.7	0.191	4.472

Note: NS = near-synchronous oscillations. Bifurcation diagram referring to boldfaced values is shown in Figure 6C.

Table 4: *Coherence Measure Values for Ten-Cell Network Simulations*

Parameters $(g_{syn}, I_\mu, \tau_{syn})$	%Het	No Noise	0.5 × SD Noise	1 × SD Noise	2 × SD Noise
(0.25,3,1) $*$	3	0.935	0.934	0.932	0.926
(0.25,3,1) $*$	8	0.372	0.366	0.331	0.331
(0.25,3,5) $*$	3	0.931	0.931	0.928	0.921
(0.25,3,5) $*$	8	0.769	0.762	0.750	0.681
(0.25,1,1) $*$	5	0.438	0.436	0.435	**0.411**
(0.25,1,1) $**$	5	0.958	0.954	0.949	**0.935**
(0.25,1,1) $*$	8	0.902	0.895	0.671	**0.436**
(0.25,1,1) $**$	8	0.906	0.903	0.893	**0.800**

Initial conditions (ICs)

$*$ - using ICs_A: $V_i = -59.5567 + \text{rand}(5.0)$ where rand() is a random number between 0 and 5 taken from a uniform distribution;

$**$ - using ICs_B: $V_i = -59.5567$.

h_i, n_i and s_i initial values are the same for ICs_A and ICs_B and are given in the Methods. i refers to the cell number, $i = 1$ - 10.

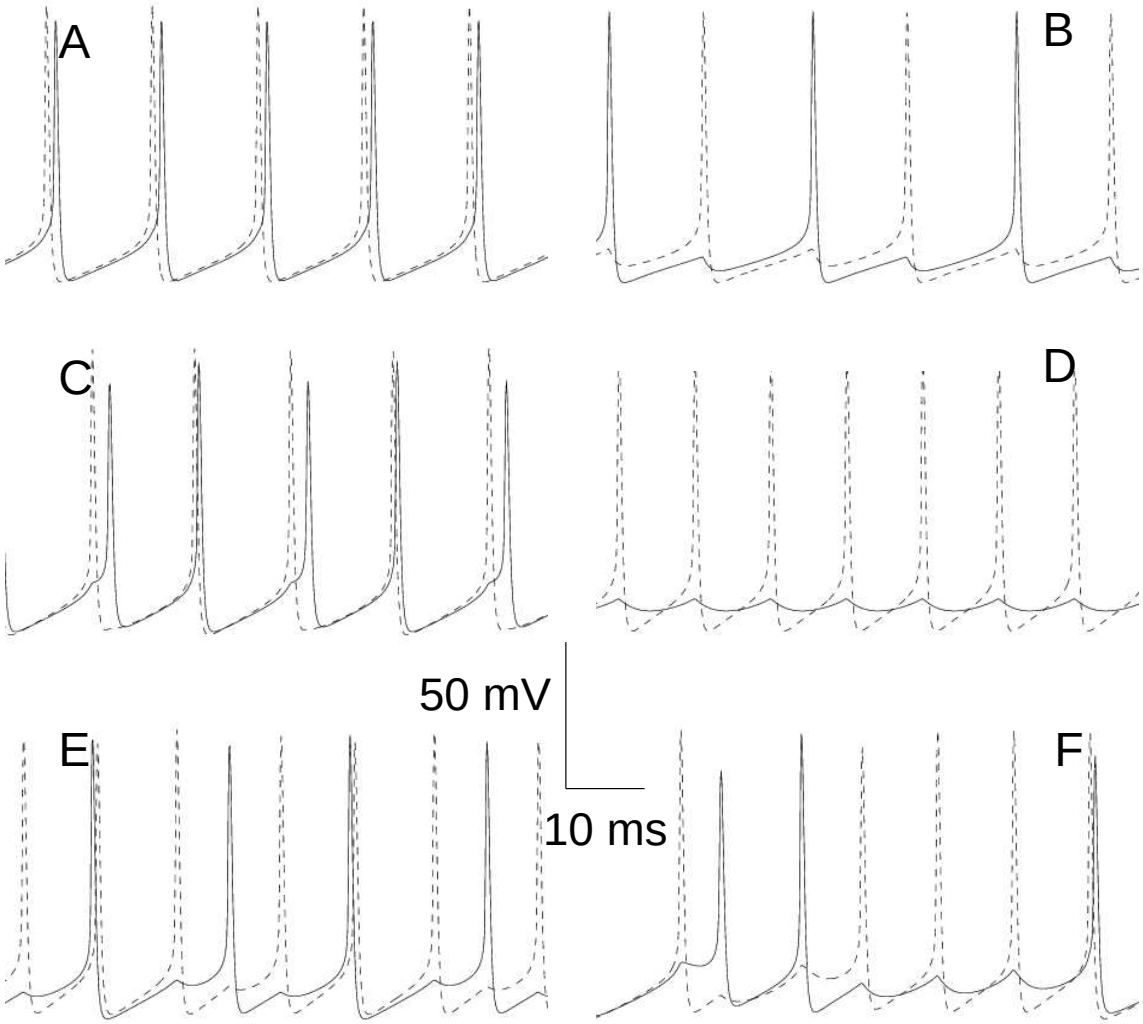

Figure 1:

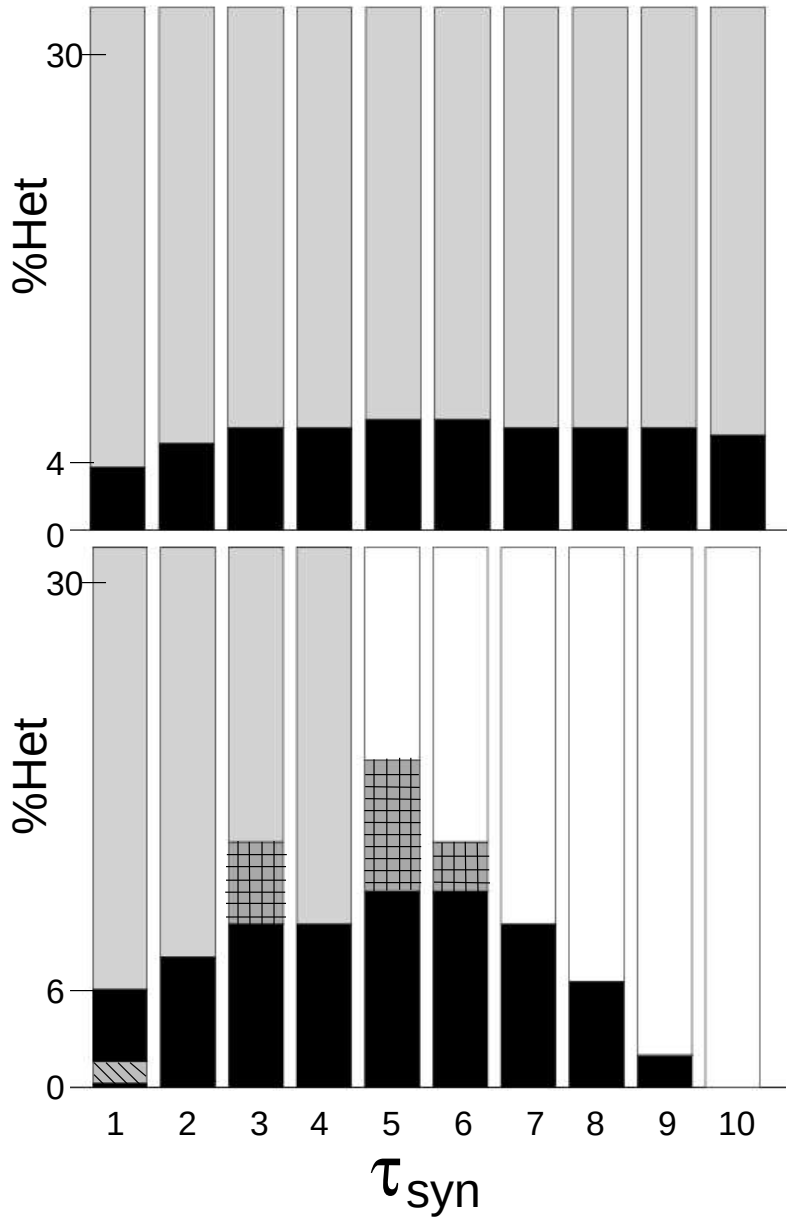

Figure 2:

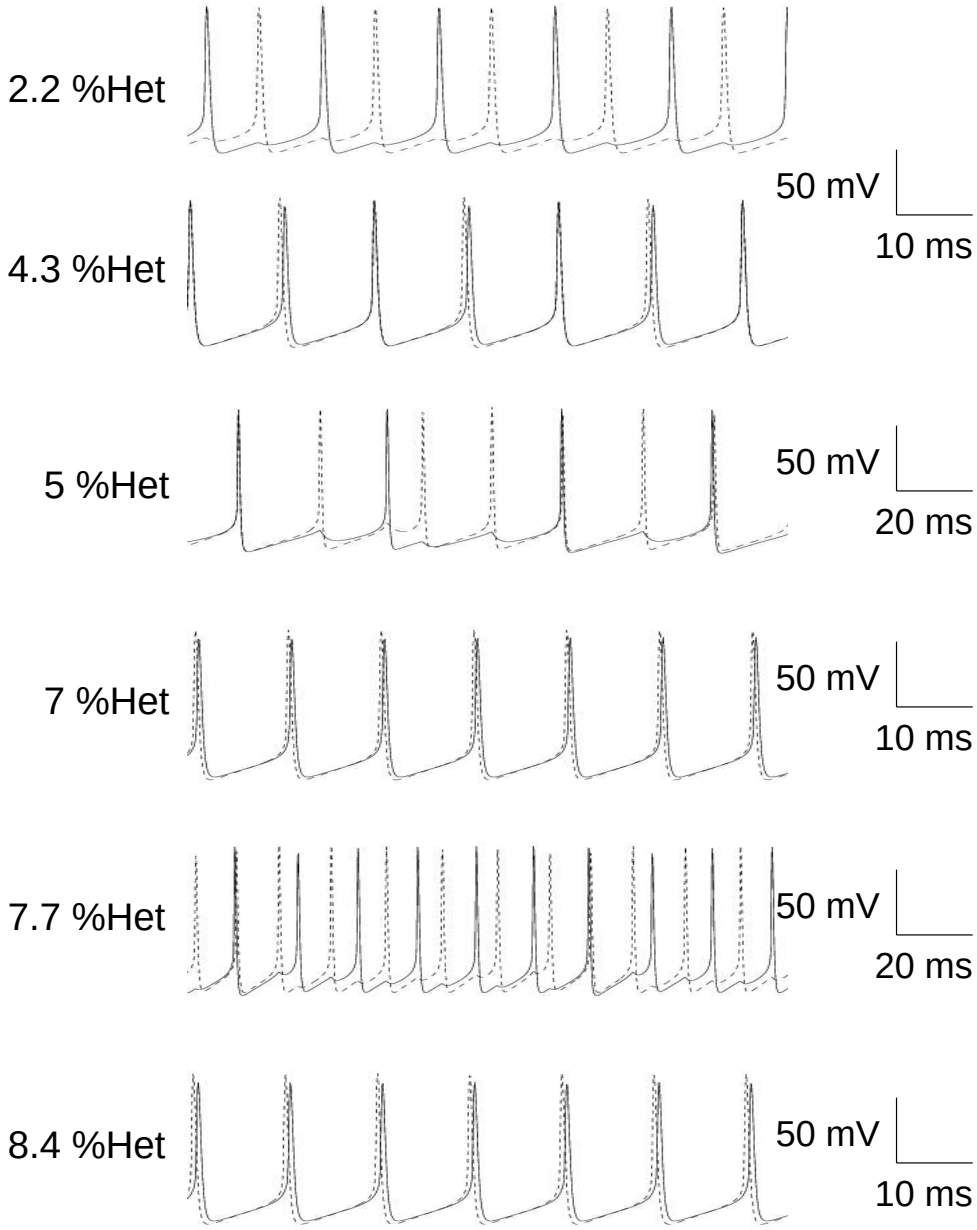
2.2 %Het
50 mV
10 ms
4.3 %Het
5 %Het
50 mV
20 ms
7 %Het
50 mV
10 ms
7.7 %Het
50 mV
20 ms
8.4 %Het
50 mV
10 ms

Figure 3:

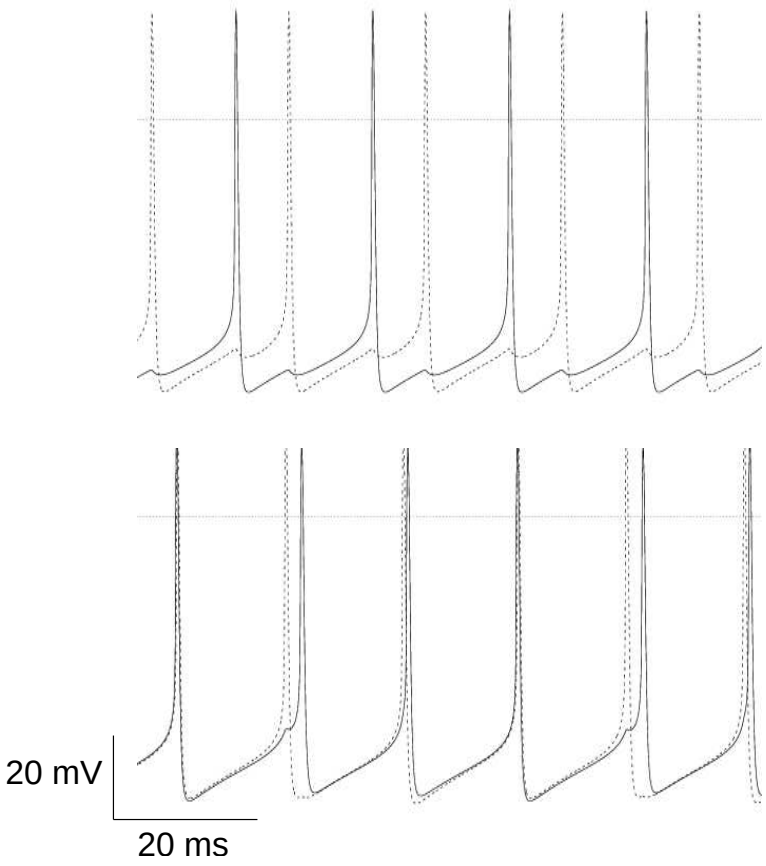

Figure 4:

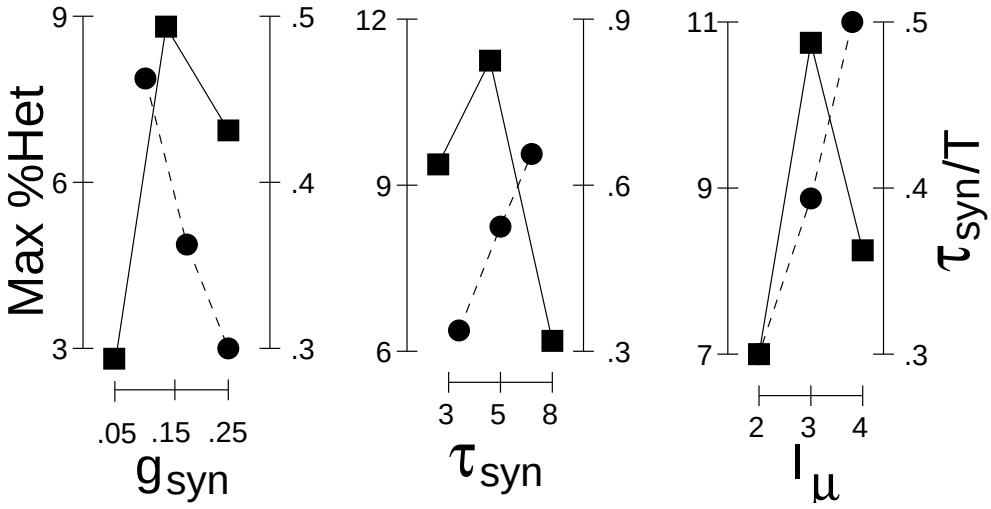

Figure 5:

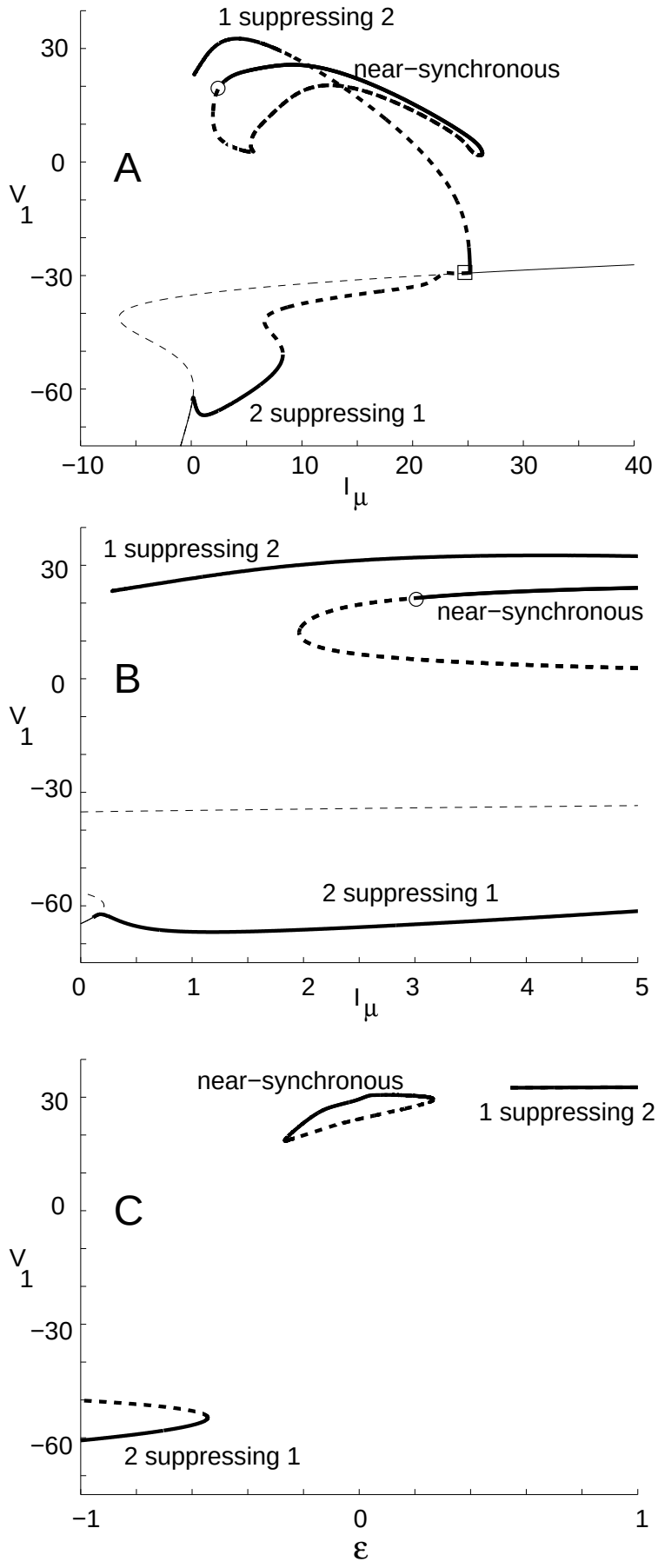
1 suppressing 2
near−synchronous
A
2 suppressing 1
V 1
I μ
1 suppressing 2
near−synchronous
B
2 suppressing 1
V 1
I μ
near−synchronous
1 suppressing 2
C
2 suppressing 1
V 1
ε

Figure 6: